Differentiation of Tumor Progression and Radiation-Induced Effects After Intracranial Radiosurgery

Mikhail F. Chernov, Yuko Ono, Kayoko Abe, Masao Usukura, Motohiro Hayashi, Masahiro Izawa, Sergey V. Diment, Pavel I. Ivanov, Yoshihiro Muragaki, Hiroshi Iseki, Tomokatsu Hori, Yoshikazu Okada, and Kintomo Takakura

Abstract A number of intracranial tumors demonstrate some degree of enlargement after stereotactic radiosurgery (SRS). It necessitates differentiation of their regrowth and various treatment-induced effects. Introduction of low-dose standards for SRS of benign neoplasms significantly decreased the risk of the radiation-induced necrosis after management of schwannomas and meningiomas. Although in such cases a transient increase of the mass volume within several months after irradiation is rather common, it usually followed by spontaneous shrinkage. Nevertheless, distinguishing tumor recurrence from radiation injury is often required in cases of malignant parenchymal brain neoplasms, such as metastases and gliomas. The diagnosis is frequently complicated by histopathological heterogeneity of the lesion with coexistent viable tumor and treatment-related changes. Several neuroimaging modalities, namely structural magnetic resonance imaging (MRI), diffusion-weighted imaging, diffusion tensor imaging, perfusion computed tomography (CT) and MRI, single-voxel and multivoxel proton magnetic resonance spectroscopy as well as single photon emission CT and positron emission tomography with various radioisotope tracers, may provide valuable diagnostic information. Each of these methods has advantages and limitations that may influence its usefulness and accuracy. Therefore, use of a multimodal radiological approach seems reasonable. Addition of functional and metabolic neuroimaging to regular structural MRI investigations during follow-up after SRS of parenchymal brain neoplasms may permit detailed evaluation of the treatment effects and early prediction of the response. If tissue sampling of irradiated intracranial lesions is required, it is preferably performed with the use of metabolic guidance. In conclusion, differentiation of tumor progression and radiation-induced effects after intracranial SRS is challenging. It should be based on a complex evaluation of the multiple clinical, radiosurgical, and radiological factors.

Keywords Differential diagnosis • Functional neuroimaging • Gamma Knife radiosurgery • Metabolic neuroimaging • Radiation-induced necrosis • Stereotactic radiosurgery • Tumor progression

M.F. Chernov (✉), M. Hayashi, Y. Muragaki, H. Iseki, and K. Takakura
Faculty of Advanced Techno-Surgery, Institute of Advanced Biomedical Engineering and Science, Tokyo Women's Medical University, 8-1 Kawada-cho, Shinjuku-ku, Tokyo 162-8666, Japan

Department of Neurosurgery, Neurological Institute, Tokyo Women's Medical University, Tokyo, Japan
e-mail: m_chernov@abmes.twmu.ac.jp

Y. Ono, K. Abe, and M. Usukura
Department of Diagnostic Imaging and Nuclear Medicine, Tokyo Women's Medical University, Tokyo, Japan

M. Izawa, T. Hori, and Y. Okada
Department of Neurosurgery, Tokyo Women's Medical University, Tokyo, Japan

S.V. Diment and P.I. Ivanov
Radiosurgical Center, International Institute of the Biological Systems, Saint Petersburg, Russia

Introduction

Stereotactic radiosurgery (SRS), particularly Gamma Knife radiosurgery (GKS) is a widely approved management option for a variety of benign and malignant intracranial neoplasms, vascular lesions, and functional brain disorders. For brain tumors, the treatment usually results in stabilization of growth, and some degree of mass volume reduction is frequently seen. Nevertheless, a number of lesions demonstrate progression after irradiation, necessitating differentiation of tumor regrowth from treatment-induced effects. Some amount of increase in the mass volume after SRS is observed in 1–10 % of pituitary adenomas and benign meningiomas [19, 61, 86], 14–70 % of vestibular schwannomas [15, 24, 62, 65],

M.F. Chernov et al. (eds.), *Gamma Knife Neurosurgery in the Management of Intracranial Disorders*, Acta Neurochirurgica Supplement, Vol. 116, DOI 10.1007/978-3-7091-1376-9_29, © Springer-Verlag Wien 2013

16–60 % of intracranial metastases [10, 18, 23, 63, 71], and 73–84 % of malignant gliomas [71]. It may reflect failure of the SRS and true progression of the neoplasm or even malignant transformation of an initially benign tumor. In the same time, regrowth may be mimicked by delayed growth arrest, temporary enlargement of the mass after low-dose radiosurgery, or radiation-induced necrosis. In some cases, formation of the new radiosurgery-induced neoplasm within the target area is suspected. It is clear that an exact diagnosis in such cases is mandatory for timely initiation of the appropriate treatment and precise determination of prognosis [30, 34].

Progressing Lesions After Radiosurgery of Intracranial Tumors

Treatment-induced changes after SRS evolve over time, and tumor progression may be initiated in varying intervals after seemingly durable initial growth control. It emphasizes the importance of close, prolonged radiological follow-up after radiosurgery, which usually comprises regular investigations with structural magnetic resonance imaging (MRI) or computed tomography (CT). These methods permit dynamic evaluation of the lesion volume, structure, contrast enhancement, degree of peritumoral edema, and mass effect. While evaluation of these parameters is useful, sometimes it cannot reliably distinguish various radiosurgery-induced pathophysiological reactions within the target. Usually decreased peritumoral brain edema and appearance of central lucency on postcontrast MRI of the lesion are considered positive prognostic factors as they indicate growth arrest and further shrinkage of both benign and malignant neoplasms [39, 54, 64]. There may also be a temporary increase in contrast enhancement of the mass with blurring or an irregular margin [39, 71], but the prognostic significance of such findings remains unknown.

In fact, even volumetric changes, which are used to assess tumor response to irradiation, are not always sufficiently predictive for a prognosis [71]. For example, up to 60 % of intracranial metastases that demonstrated varying degrees of volume reduction soon after radiosurgery enlarged thereafter [23]. However, in 20–64 % of cases it is not caused by tumor regrowth due to treatment failure but by radiation-induced effects [23, 30, 32, 71], and even histopathological investigation after surgical resection of these lesions could not reveal viable neoplastic tissue. According to Huang et al. [30], a 65 % increase in the volume of a metastatic brain tumor after irradiation represents the best threshold for identifying recurrence. However, it has only 80 % specificity, which fell to 50 % for lesions irradiated with a biological effective dose (BED) of >200 Gy (approximately 19 Gy of marginal dose delivered at a single session) [30]. In the series of Essig et al. [17], volumetric changes in intracranial metastases at 6 weeks after SRS had just 64 % positive prediction value (PPV) and 43 % negative prediction value (NPV) for overall response to treatment.

Regrowth of the Intracranial Tumors due to Treatment Failure

Failure of radiosurgery to control the intracranial tumor may be caused by suboptimal targeting, insufficient treatment dose, and/or resistance of the neoplasm to irradiation, particularly due to prominent malignant growth potential. Inability to identify clearly the borders of the mass on conventional neuroimaging is considered one of the main reasons for SRS failure in such different tumors as adrenocorticotropic hormone-secreting pituitary adenomas and gliomas. Intentionally decreasing the radiation dose delivered to the target because of its large volume or critical location may be the main reason of regrowth of schwannomas and meningiomas after sterotactic irradiation [86]. Radiosurgery has limited effectiveness for malignant extracerebral intracranial tumors, especially if applied as salvage treatment at the time of evident tumor progression. Some brain metastases (e.g., those originating from sarcomas, colon and renal carcinomas, and malignant melanoma) are relatively resistant to SRS and may require greater radiation doses [38].

Malignant Transformation of Benign Intracranial Tumors

Malignant transformation of benign brain tumors after GKS is uncommon. In fact, it can be easily mistaken with spontaneous dedifferentiation, particularly if irradiation is performed at the time of regrowth or recurrence after initial lesion resection [48, 58]. Moreover, in some of such cases reexamination of the tissue specimen obtained at the time of surgery may reveal missed features of anaplasia [48]. It should be borne in mind that rare malignant subtypes of schwannomas and meningiomas can be radiologically indistinguishable from their typical benign counterparts. Thus, their progression, despite SRS, is easily confused with malignant transformation. Kubo et al. [48] analyzed 11 such cases after SRS or radiotherapy of vestibular schwannomas and found that in 7 of them irradiation was applied as a primary treatment modality without detailed examination of the neoplastic tissue, and 5 patients had neurofibromatosis type 2, which has known association with a high risk of malignancy. It should be

noted that in rare cases accelerated growth of benign tumors was observed during various time periods after SRS, but tissue investigation after subsequent resection usually confirmed preservation of the benign histopathological pattern [14].

Delayed Growth Arrest and Temporary Enlargement of Benign Brain Tumors

Stabilization of growth with or without subsequent shrinkage is the most typical outcome after low-dose SRS for benign intracranial tumors. However, other patterns of volumetric response to irradiation are not uncommon. Temporary enlargement of the irradiated neoplasm has become a recognizable clinical phenomenon, which is rather typical for slow-responding masses [64]. It usually does not reflect true tumor progression and only infrequently requires additional treatment.

Several months after radiosurgery 14–70 % of vestibular schwannomas demonstrate an increase in their volume [15, 24, 62, 65], which constitutes in median 75 %, although it may reach 200 % [15, 65]. Regarding linear measurements, the tumors may increase >5 mm in one axis [15, 65]. Hasegawa et al. [24] noted that such changes were more common in women with large, particularly cystic neoplasms. Temporary lesion enlargement may be more frequent after irradiation with higher doses as it was noted in 70 % of patients treated before introduction of low-dose SRS for benign intracranial tumors [62]. The phenomenon may be more profound in nonvestibular, particularly trigeminal, schwannomas [55]. Increased mass volume is usually accompanied by loss of central contrast enhancement on T1-weighted MRI, also known as the "black hole" [54]. The pathophysiological mechanism remains the subject of debate, but delayed growth arrest, radiation-induced necrosis, and/or apoptosis with inflammation and swelling are considered the main causes. Histopathological investigation may reveal parenchymal necrosis, thickening of the vascular walls as a result of endothelial and pericytic proliferation, perivascular infiltration of macrophages and small lymphoid cells, thrombus formation, and foci of minute hemorrhages [24, 26, 48]. Appearance of new symptoms, particularly hemifacial spasm, was noted in 20 % of patients, but they are usually self-limiting or resolve with steroid therapy [65].

The most important fact, which is clearly recognized at present, is that more than half of vestibular schwannomas exhibiting enlargement after SRS demonstrate shrinkage later on, whereas many others have growth stabilization without further progression. The appearance of central lucency on contrast-enhanced images is usually followed by reenhancement, and considered a favorable factor for further volume regression [24, 54, 64]. In such cases, residual inactive lesions with prominent fibrotic changes usually appear as small contrast-enhanced masses within the target area, resembling a "white dwarf" [54]. Only in 2–7 % of patients undergoing GKS for a vestibular schwannoma, serial neuroimaging demonstrates continuous tumor progression, cystic degeneration, or enlargement of preexisting cysts, which necessitates additional treatment with surgery or repeat radiosurgery [24, 65].

Similar volumetric changes are sometimes observed after low-dose radiosurgery of other benign tumors [19, 61, 62, 64]. In the series of Feigl et al. [19], around 3 % of World Health Organization (WHO) grade I meningiomas demonstrated an initial volume increase after GKS followed by shrinkage or growth stabilization. Pamir et al. [61] noted some enlargement of pituitary adenomas 3–9 months after GKS, although their size subsequently decreased in all cases. This phenomenon was also noted after SRS of a low-grade glioma [64].

Radiation-Induced Necrosis

Radiation-induced necrosis is a well-known phenomenon, mimicking brain tumor progression after irradiation. It corresponds to early-delayed or late injury and usually develops several months to several years after treatment, while clinical manifestation was occasionally reported even 13 years after SRS [7]. The incidence of symptomatic radiation-induced necrosis after intracranial radiosurgery varies in most series from 2 % to 14 %. Its risk is directly associated with greater radiation doses, radiation energy delivered to the target, prescription isodose volumes, 10 Gy and 12 Gy irradiation volumes; larger number of isocenters; tumor dose inhomogeneity; lower selectivity of the treatment plan; previous administration of SRS or radiotherapy; longer duration of follow-up [3, 5, 13, 20, 21, 32, 42, 47, 63, 64]. Radiation injury is rarely observed after low-dose treatment of benign neoplasms. The type of pathology is important: In the series of Chin et al. [13], the incidence of the complication after GKS was 17 % for gliomas but 6 % for other tumors. The development of radiation injury is a complex process, and it is difficult to predict its probability based on the limited number of clinical and radiosurgical parameters. It may be predisposed in some way by individual radiosensitivity [13, 21, 63] and specific medical conditions (e.g., diabetes), be more pronounced in well-oxygenated tissues [42], and be confounded by adjuvant and concurrent chemotherapy [5, 34].

The underlying pathophysiological mechanisms include initial direct cellular damage and microvascular injury with progressive thickening of the large vessel walls caused by hyalinization leading to thrombosis, infarction, and necrosis. Correspondingly, the most common histopathological findings in such cases are fibrinoid necrosis of the vascular

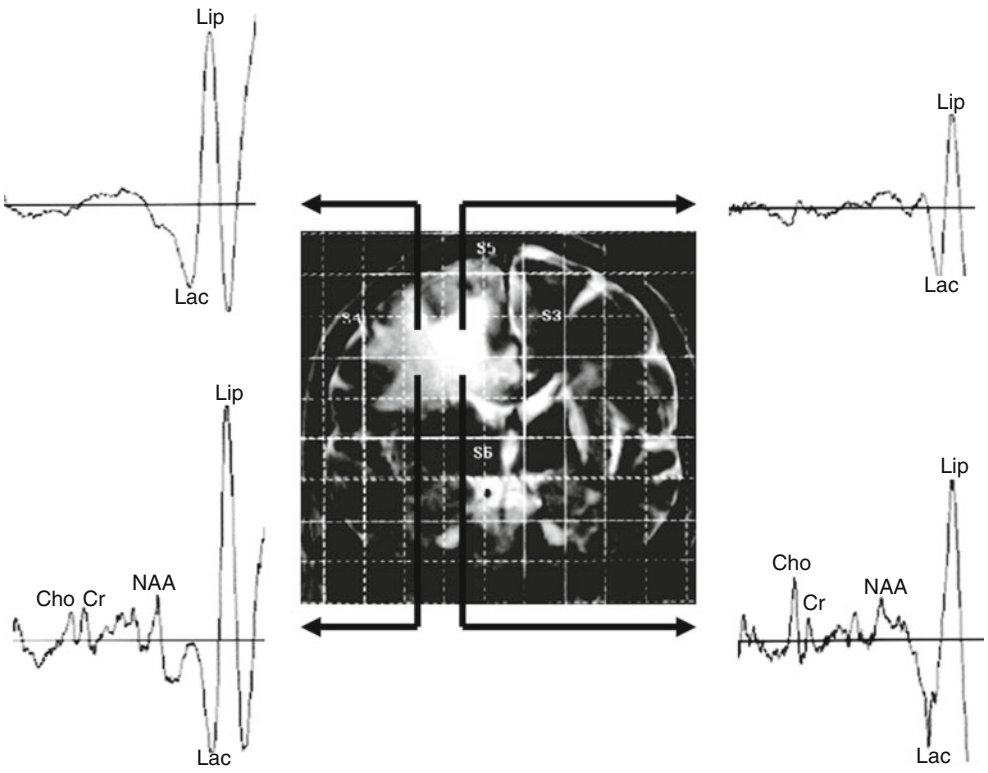

Fig. 1 Multivoxel proton magnetic resonance spectroscopy (^{1}H-MRS) in a case of radiation-induced necrosis of the peritumoral brain after Gamma Knife radiosurgery (GKS) of a metastatic brain tumor. Note the presence of a necrosis pattern in spectroscopic voxels containing brain tissue adjacent to the target. *NAA N*-acetylaspartate, *Cho* choline-containing compounds, *Cr* creatine, *Lac* lactate, *Lip* mobile lipids (*Source*: Chernov et al. [12])

walls with degradation of their basement membranes, endothelial damage with proliferation of endothelial cells and fibroblasts, vessel dilatation, telangiectasia, and perivascular infiltration of lymphocytes, plasma cells, and macrophages [7, 26, 34]. There is widespread permeation of the tissue by fibrin caused by increased permeability of the vessels [42]. Also, irradiation alters fibrinolytic enzyme activity and initiates the immune response, which may cause autoimmune vasculitis [34]. Other changes include minute hemorrhages, calcifications, fibrosis, and cyst formation [5, 26]. Microvascular proliferation in necrotic foci or in their vicinity is seen in some cases [26]. In the perilesional brain loss of oligodendrocytes, which are extremely sensitive to irradiation, leads to demyelination, whereas increased vascular permeability results in vasogenic brain edema; astrocytosis and shrunken neurons associated with local brain atrophy are seen subsequently [39, 70].

Unlike the tissue necrosis caused by wide-field radiotherapy, after SRS the radiation injury is usually localized and well restricted. In general, it is important to differentiate radiation-induced tumor necrosis and radiation-induced necrosis of the peritumoral brain [12]. Both conditions present as diffuse signal hyperintensity on T2-weighted images that exceed the target area. They are sometimes characterized as "supernovas" [54], and usually accompanied by perilesional contrast enhancement due to blood–brain barrier (BBB) disruption [62, 64]. Nevertheless, with radiation-induced tumor necrosis, the changes in the adjacent brain parenchyma are mainly caused by diffusion of metabolically active substances (i.e., cytokines) from the damaged neoplasm. Therefore, this condition is frequently reversible, although it may require surgical resection of the mass [64]. Hence, radiation-induced tumor necrosis may be considered a more or less acceptable side effect after radiosurgery of malignant lesions [13]. In contrast, radiation injury to the peritumoral brain caused by excessive radiation is an avoidable complication as it is usually due to suboptimal targeting with low selectivity (Fig. 1).

Table 1 Histopathological classification of radiation treatment effects on tumors (modified from Ohoshi and Shimosato)

Grade	Histopathological characteristics
0	No radiation effect
I	Cellular damage without destruction of tumor clusters
II	Cellular damage with destruction of tumor clusters
III	Nonviable tumor cells
IV	No tumor cells (including coagulation necrosis)

Source: Kamada et al. [38]

The main diagnostic and treatment challenges posed by intracranial lesion progression after radiosurgery and radiotherapy are related to their common histopathological heterogeneity, the nearby coexistence of a viable tumor, and radiation-induced changes (Table 1), which may be particularly evident at the periphery of the target [38]. Such findings were identified in 35–74 % of brain metastases and nearly

100 % of high-grade gliomas that underwent surgical resection after initial SRS [16, 32, 40, 41, 71]. They are also observed in some extracerebral intracranial neoplasms [48].

Presenting symptoms and clinical behavior of radiation-induced necrosis vary significantly. Incidental, self-limiting, steroid-controlled, progressive, and recurrent forms are well recognized [3, 7, 44, 47]. Space-occupying lesions resistant to medical therapy may require surgical resection [20, 40, 64]. Milder forms are mainly related to edema resulting from BBB disruption and demyelination. Hence, their radiological definition as "radiation-induced enhancement" (not "necrosis") might be more correct, at least at the early stages of development [42, 66]. Extensive radiation-induced necrosis and cyst formation may be observed after radiosurgical management of nonneoplastic pathology, such as an arteriovenous malformation (AVM) and cavernomas, which sometimes requires differentiation from new tumor formation [7, 20].

New Tumor Formation

There is no evidence that SRS increases the risk of malignancy, and formation of new radiosurgery-associated tumors is exceptionally rare [53, 72]. The roughly estimated risk is <0.001 % [58]. In 2009, Niranjan et al. [58] identified nine reported cases that met standard Cahan's criteria for radiation-induced neoplasms: four glioblastomas, one anaplastic astrocytoma, three meningiomas, and one vestibular schwannoma. The complication manifested within 5–16 years after SRS for benign brain tumors (four cases), malignant melanoma metastases (one case), and AVM (four cases).

Differentiation of the Tumor Regrowth and Radiation-Induced Effects After Radiosurgery

Various clinical and radiosurgery-related characteristics (e.g., histopathological type of the lesion, its volume, previously applied SRS or radiotherapy, radiation dose and its distribution, dynamics of symptoms, time elapsed until identification of progression) should be certainly taken into consideration during differentiating tumor regrowth from radiation-induced effects. However, such parameters are quite similar in both clinical entities and their assessment alone rarely establishes a clear diagnosis [30, 81]. Barajas et al. [2] reported that intraaxial metastatic tumors that later recurred had a trend to have larger volume and lower prescribed doses at the time of irradiation, although the differences were not statistically significant. Kano et al. [41] found that a shorter interval between GKS of brain metastasis and subsequent resection necessitated by lesion progression was associated with a greater incidence of finding viable neoplasm in the histopathological specimen. In concordance, Kihlstrom and Karlsson [42] noted that a tumor recurrence after radiosurgery is more likely during the first posttreatment year, whereas radiation injury is usually delayed. However, these temporal interrelations were not confirmed by others [2, 12, 27, 33, 56]. Our series of patients with intracranial metastases progressing after GKS included 11 cases of pure tumor recurrence or regrowth, 10 cases of pure radiation-induced tumor necrosis, and 11 cases of mixed lesions. None of the clinical and radiosurgical parameters (including location and initial volume of the intracranial neoplasm, previous irradiation by means of SRS or fractionated radiotherapy, maximum and marginal irradiation doses, initial volumetric tumor response after radiosurgery, time to deterioration) differed significantly between the groups [12]. Therefore, it is evident that various neuroimaging modalities must play the main diagnostic role in such cases.

Historical Methods (Angiography and Scintigraphy)

Attempts were made in the past to use cerebral angiography to differentiate tumor recurrence from radiation-induced necrosis, but the results were generally nonspecific [4, 5]. Currently, its use in such cases has been practically abandoned, although it represents the gold standard for evaluating AVMs after radiosurgery. Similarly, scintigraphy and tomoscintigraphy with such tracers as sodium pertechnetate, DTPA technetium, and iodoamphetamine (IMP) were widely performed before introduction of the contemporary neuroimaging modalities, but frequent false-positive and false-negative results were noted [5].

Structural CT and MRI

At the time of lesion progression after radiosurgery, CT has limited opportunities for differentiating tumor regrowth from radiation-induced necrosis because both conditions typically appears similarly as a contrast-enhancing low-density mass within the target area surrounded by brain edema and frequently associated with a mass effect [4, 5, 42, 45]. According to our experience, neither the lesion volume nor extent of the perilesional edema differs significantly in cases of pure tumor recurrence, pure radiation-induced necroses, and mixed pathology after GKS of intracranial metastases, whereas a midline shift at the time of clinical deterioration was relatively more common in cases of radiation injury [12].

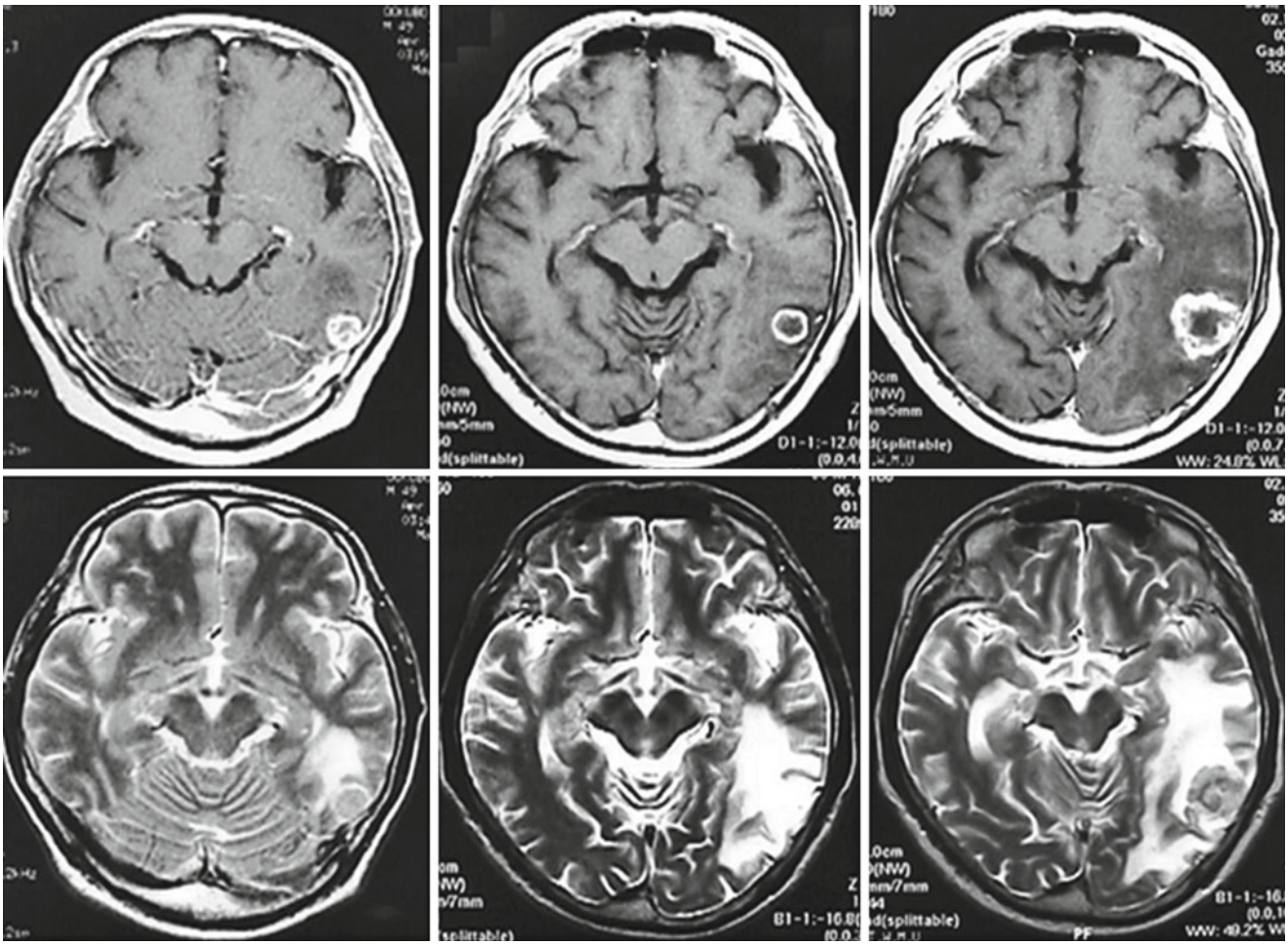

Fig. 2 Dynamics of the structural changes in a metastatic adenocarcinoma of the lung after GKS. At 1 month after treatment the size of the lesion had not changed significantly, although there was the appearance of a central lucency without any corresponding hypointense areas on T2-weighted images. At 10 months after treatment, there was a significantly increased heterogeneously enhanced lesion that well corresponded to the hypointense area on T2-weighted magnetic resonance imaging (MRI) on the background of a hyperintense signal caused by brain edema. Histopathological investigation after subsequent resection revealed mixed pathology with coexistent viable tumor and radiation-induced necrosis

On the other hand, structural MRI may provide some useful diagnostic information. Particularly helpful for identifying tumor regrowth is an evaluation of the correspondence of the target-related hypointense area on the background of the hyperintense signal on T2-weighted MRI to the contrast-enhanced lesion on T1-weighted MRI. It is defined as the lesion quotient or a T1/T2 match/mismatch [16, 40, 41]. The greater the correspondence of their cross-sectional areas to each other, the higher is the probability that a progressing tumor is present (Fig. 2). Dequesada et al. [16] reported that in all seven patients with histopathologically confirmed pure neoplastic pathology, this ratio was ≥0.6, and use of its cutoff level at 0.3 predicted the presence of a viable neoplasm in 26 of 27 cases. The reported sensitivity and specificity of a T1/T2 match for identifying recurrent brain metastases after GKS are 94 % and 77 %, respectively [40]. On the other hand, an indistinct hypointense lesion on T2-weighted MRI that failed to correlate with the T1-weighted contrast-enhanced volume was significantly associated with detection of pure necrotic changes in the tissue specimens. However, viable neoplastic elements were identified in 33 % of contrast-enhanced masses that did not have any corresponding hypointense area on T2-weighted images [40, 41].

Other features associated to some degree with progression of metastatic brain tumors after irradiation can be also identified on MRI: arteriovenous shunting, gyriform distribution of the hyperintense area corresponding to lesion and perilesional edema on T2-weighted images, cyst formation, and marginal or solid contrast enhancement [16]. On the other hand, some specific forms of contrast enhancement (Fig. 3), defined as “cut green pepper” (multiple irregular rings of enhancement), “Swiss cheese/soap bubble”

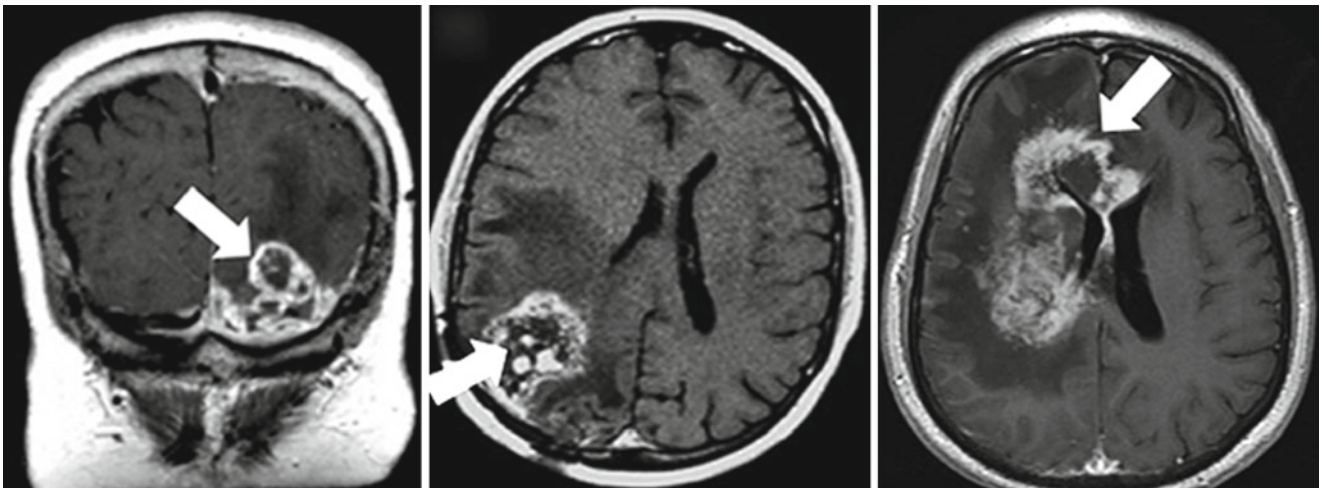

Fig. 3 Specific forms of contrast enhancement (*arrows*) typical for radiation-induced necrosis: "cut green pepper" (*left*), "soap bubble" (*center*), and "spreading wavefront" (*right*) (*Sources*: Dequesada et al. [16], Rogers et al. [70], and Jain et al. [34])

(multiple small or moderate-sized areas of enhancement intermixed with foci of necrosis), and "spreading wavefront" (blurred margin of enhancement) are considered more typical, although not highly specific, of radiation-induced necrosis [16, 34, 57, 70]. Overall, structural MRI is somewhat helpful in cases of parenchymal brain lesions progressing after irradiation, but the information provided usually is not enough for a precise diagnosis. There is general agreement that additional functional and metabolic radiological investigations are mandatory [22, 25, 34, 39, 59, 60, 66].

Diffusion-Weighted Imaging and ADC Mapping

Diffusion-weighted imaging (DWI) reveals microscopic Brownian motion in tissue water, and the apparent diffusion coefficient (ADC) quantitatively describes the effective mean diffusivity, which is determined by the tissue cellularity, viscosity of the medium, and spacing of the diffusion barriers. Highly cellular brain tumors usually appear on DWI as hyperintense lesions and have a low ADC. Treatment-related calcifications, gliosis, or fibrosis in the mass may influence the intensity of the signal. Of note: the ADC of brain tumors is relatively insensitive to steroid therapy, which facilitates use of DWI during posttreatment follow-up [84].

In contrast, a hypointense signal on DWI and high ADC are considered typical of radiation-induced necrosis [1, 22, 23, 31, 39], which may, however, exhibit a variety of signal patterns [66]. Particularly, necrosis with a viscous mucinous component may appear on DWI as a hyperintense lesion and have low ADC values, similar to brain abscesses [66]. A low ADC can also be caused by an inflammatory cellular composition at the early stages of radiation injury and by the presence of hemorrhages. Probably for these reasons direct comparison of ADC led to controversial results because higher values for both radiation injury [1] and tumor recurrence [75] were reported. In mixed lesions evaluation of the spatial heterogeneity of ADC by means of "diffusion mapping" may allow to define presence of tumor recurrence adjacent to necrotic areas [1, 22, 31].

Diffusion Tensor Imaging

The basic principles of diffusion tensor imaging (DTI) are similar to those of DWI except that DTI evaluates the directionality and magnitude of water diffusion characterized by fractional anisotropy (FA). FA was found to be slightly higher, whereas the FA ratio (FA values normalized by region-of-interest [ROI] in the contralateral white matter) was significantly higher in normal-appearing white matter adjacent to the perilesional edema in patients with treatment-related injury after radiochemotherapy of intracranial gliomas compared to patients with recurrent neoplasms [75]. Additionally, eigenvalues and the principal eigenvalue ratio were significantly higher in contrast-enhancing lesions in a group of patients with recurrence [75]. Thus, DTI may be somewhat helpful in differenting radiation-induced necrosis from regrowth of a brain neoplasm after SRS, at least for infiltrative gliomas, which justifies further research in this area [84].

Perfusion CT and MRI

At present, the hemodynamics of intracranial neoplasms can be evaluated in vivo with perfusion CT and MRI using first-pass dynamic susceptibility-weighted contrast-enhanced perfusion imaging or arterial spin labeling. Various

parameters determined by these techniques, including cerebral blood flow (CBF), cerebral blood volume (CBV), mean transit time (MTT), relative peak height (PH), percentage of signal-intensity recovery (PSR), contrast transfer coefficient (K^{trans}), allow detailed characterization of the lesion's microvascularity and the permeability of its vessels. They can be applied effectively to differentiate tumor progression from radiation-induced changes.

Increased neoangiogenesis and vascular density are characteristic features of most neoplasms, especially those that are malignant. Typically, CBV is greater in recurrent high-grade brain masses than in white matter and lower or equal to that in gray matter [27]. Its maximum values correspond to intralesional areas of increased mitotic activity [66]. Because effective irradiation alters the blood supply of the tumor, low CBV and CBF and increased MTT are usually seen in radiation-induced necrosis [2, 22, 34, 35, 66]. However, sometimes the contrast-enhanced component of the necrotic lesion has greater perfusion than is seen in white matter, probably owing to the relatively increased density of capillaries in the areas of inflammation, or to extension of the vascular lumen caused by telangiectasia and dilatation of the blood vessels [2, 33, 34, 66]. Of interest, several studies from various centers [27, 30, 56] determined similar optimal thresholds of the relative CBV (normalized to white matter) for identifying recurrent intracranial metastasis after irradiation: Its value of ≥2.0 proved to have 70–96 % diagnostic accuracy (Fig. 4). However, for gliomas the cutoff level may be lower: Jain et al. [35] used perfusion CT to investigate the optimal threshold of the relative CBV for identifying a progressing tumor, and determined that it was 1.65 providing 83 % sensitivity and 100 % specificity.

The perfusion abnormalities in tumors are related not only to the large number of neoplastic vessels but also to their abnormal characteristics, such as increased permeability, which may be detected in recurrent neoplasms and used for their diagnosis [2, 33, 34]. In the multivariate analysis performed by Jain et al. [33], the permeability surface area product and the relative CBV showed independent significant association with differentiating between the groups of regrowing tumors (mainly gliomas) and treatment-induced necrosis. Of note: Vascular leakiness in patients with a radiation injury is also increased because of the damaged endothelium and hypoxia-related up-regulation of vascular endothelial growth factor (VEGF), but its magnitude is less than that of viable high-grade neoplasms [33].

Perfusion CT provides robust data and better options for quantitative analysis because of the linear relation between the contrast agent's concentration and tissue attenuation. However, radiation exposure and use of relatively large volumes of iodinated contrast medium limit its utility for assessing brain tumors [33–35, 56]. On the other hand, perfusion MRI provides better anatomical resolution but is susceptible to multiple technical and methodological errors, and its results may be significantly affected by some pathophysiological characteristics of the investigated tissue [2, 34]. Artificially increased hemodynamic parameters are obtained if the examination is performed in the vicinity of major vascular structures [66]. Also, the presence of hemorrhage, melanin depositions, cysts, or significant extravasation of contrast medium in the investigated area may produce susceptibility artifacts and lead to erroneously decreased CBV values in the viable neoplasm [2]. Inaccurate estimation of CBF and CBV may be caused by BBB alteration as interstitial edema may compress the small vessels [33–35, 83]. In addition, the tumor vasculature is sometimes significantly compromised by rapid growth with necrotic changes [34, 35]. Low spatial resolution of the method may challenge a precise diagnosis in the presence of mixed lesions with a coexistent viable neoplasm and radiation injury, although creation of "perfusion maps" may resolve this problem [34, 35, 66]. Finally, the results of perfusion studies are significantly affected by administration of steroids or antiangiogenic therapy (e.g., bevacizumab), which is currently used for management of both recurrent parenchymal brain tumors and radiation-induced necrosis [34, 84].

Proton Magnetic Resonance Spectroscopy

Proton magnetic resonance spectroscopy (^{1}H-MRS) allows noninvasive biochemical characterization of human tissue located within the predefined voxel. The method is intrinsically multiparameter and permits simultaneous evaluation of the variety of metabolites, which in the human brain usually includes *N*-acetylaspartate (NAA), choline-containing compounds (Cho), creatine (Cr), lactate (Lac), and mobile lipids (Lip). These metabolites are associated with rather specific histopathological and pathophysiological properties of the investigated tissue (Table 2). In the clinical setting, the content of metabolites is frequently expressed semiquantitatively, as various ratios.

^{1}H-MRS showed high effectiveness for differentiating a recurrent tumor from radiation-induced necrosis. In such cases, use of a multivoxel investigation (also known as spectroscopic or chemical shift imaging) is particularly important because it provides the optimal spatial resolution required for distinguishing the coexistent viable neoplasm from treatment-induced changes [11, 49, 66]. Our study showed 100 % diagnostic accuracy of this method in cases of intracranial metastases enlarging after GKS [11]. The tumor is usually characterized by an elevated Cho peak, decreased NAA and Cr peaks, and frequent appearance of Lac and Lip peaks [10, 25, 49, 51, 84]. The two latter metabolites

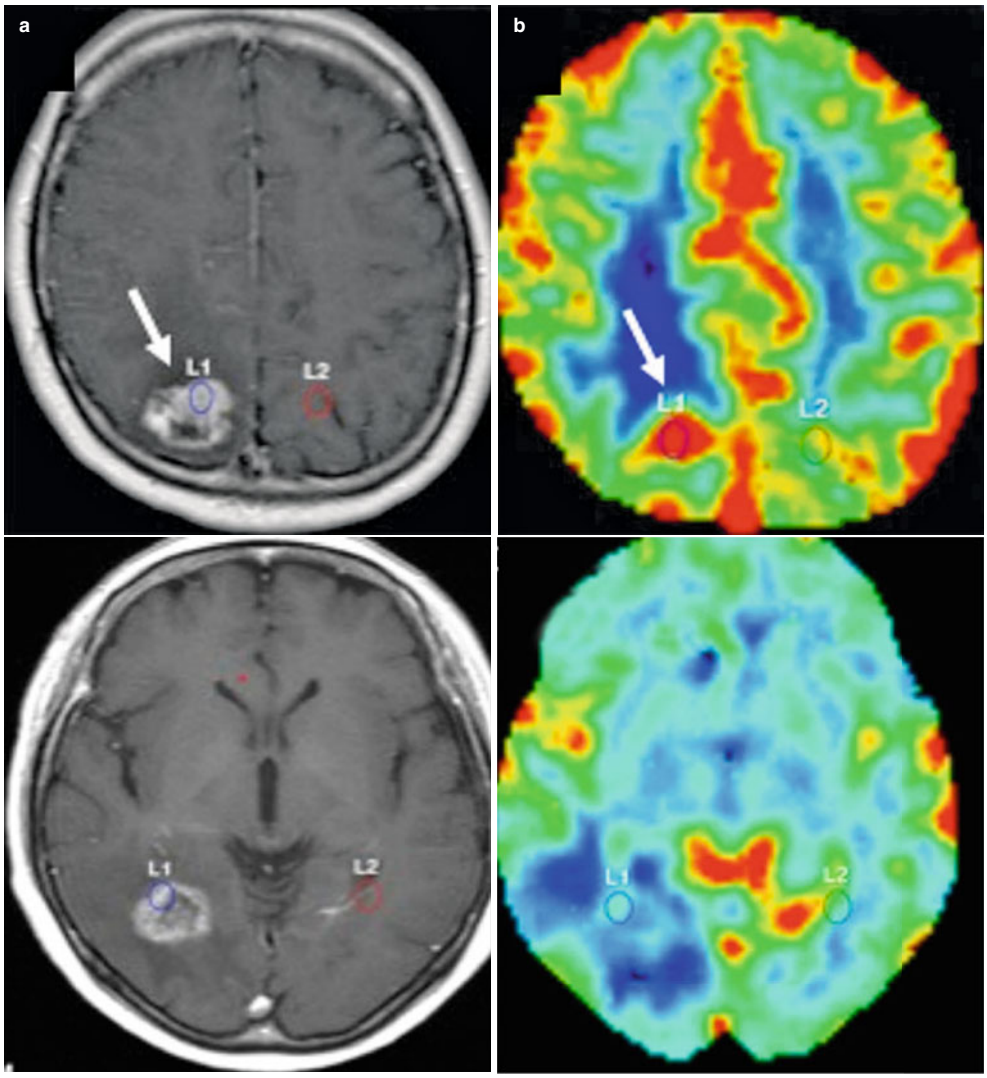

Fig. 4 Contrast-enhanced T1-weighted (**a**) and perfusion-weighted (**b**) MRI in cases of tumor recurrence (*upper*) and radiation-induced necrosis (*lower*) after radiosurgery of metastatic brain tumors. Note the clear difference in the cerebral blood volume of lesions (*Source*: Mitsuya et al. [56])

predominate on the spectrum of necrotic lesions, although in some of such cases no reliable peaks can be identified at all. However, in cases of early radiation-induced injury, Cho may be elevated because of inflammation, demyelination, and gliosis, and the spectroscopic pattern may resemble that of a tumor [49, 66, 84].

The list of proposed thresholds of different metabolic ratios for identifying a recurrent tumor is endless. It includes Cho/Cr >2.5 [43, 44, 51], Cho/Lip + Lac >0.3 [44], and Cho/nCho >1.2 [30] after SRS of brain metastases; and Cho/NAA >1.8 [75], Cho/Cr >1.8 [75], Cho/nCr >1.79 [68], and Lip + Lac/Cho <0.75 [68] after radiochemotherapy of intracranial gliomas. In our experience, the combination of NAA/Cho ratio <1 and Lip/Cho ratio <3 in at least one lesion-containing voxel of multivoxel ^{1}H-MRS showed high diagnostic accuracy for identification of regrowing brain metastases after GKS, and corresponded well to the histopathology in a surgically treated cases [11, 12]. It should be kept in mind that evaluated metabolite ratios have variability of, at least, 10–15 %, whereas technical differences of processing and postprocessing during spectroscopic examinations significantly complicate comparison of results obtained on different MRI scanners. Hence, additional pattern analysis of the ^{1}H-MR spectra can be helpful (Fig. 5).

In the series of patients with gliomas, Rock et al. [68, 69] found that spectroscopic imaging allows reliable differentiation between pure tumor and pure radiation-induced necrosis, but the distinction is less definitive for mixed lesions. Possible false-negative results of ^{1}H-MRS in the determination of recurrent neoplasms may be caused by the relatively large size of the spectroscopic voxel (usually ≥1 cm^{3}), incomplete coverage of the lesion, and/or the inability to differentiate between radiation-induced and tumor-induced necrosis. Some tumors, such as intracranial metastases of colorectal carcinoma, may have extremely high Lip content, which may complicate their differential diagnosis. Finally, the presence of hemorrhage in the investigated volume of tissue and location of the mass in the vicinity of cerebral

Table 2 Role of specific ^{1}H-MRS-detected metabolites in brain tissue characterization

Main ^{1}H-MRS-detected metabolites in human brain	Histopathological and pathophysiological correlates
N-Acetylaspartate (NAA)	Extremely sensitive axonal and neuronal marker that reflects their density, viability, and functional activity. Nonspecific decrease accompanies nearly all brain dysfunctions.
Choline-containing compounds (Cho)	Associated with both synthesis and degradation of cell membranes. Elevated in areas with increased proliferative activity, high cellularity, inflammation, and early necrosis. Decrease is associated with cell loss.
Creatine (Cr)	Reflects energetic properties of the investigated tissue. Usually, but not always, decreased in brain tumors. Frequently used as internal standard for evaluating the other metabolites' content.
Lactate (Lac)	Usually not detected in normal brain. Appears in areas of increased glycolysis, anaerobic metabolism, ischemia, or impaired mechanisms of lactate utilization.
Mobile lipids (Lip)	Usually not detected in normal brain. Appears in areas with high rate of cell membrane turnover, tissue breakdown, and necrosis.

^{1}*H-MRS* proton-magnetic resonance spectroscopy

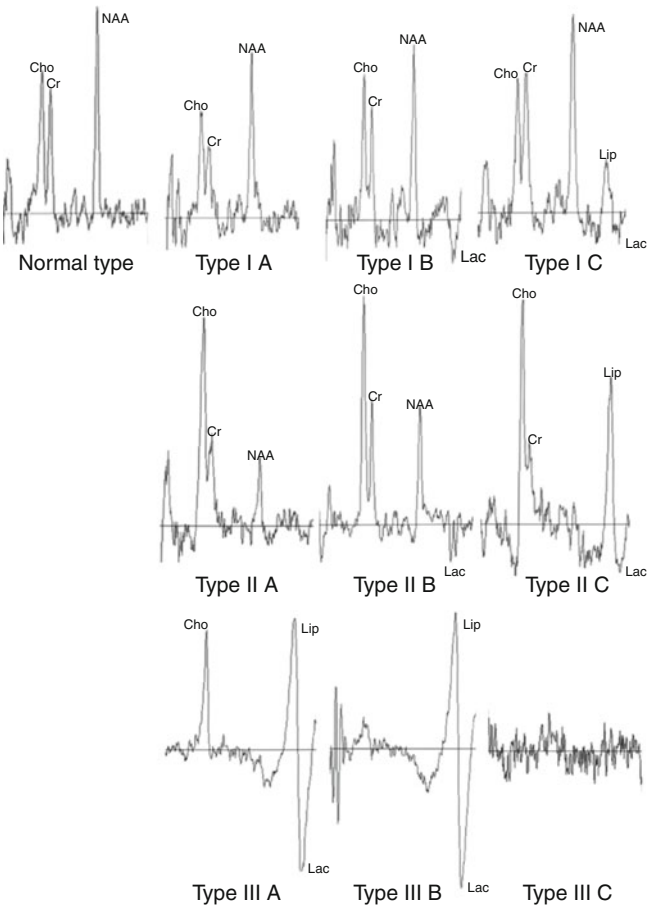

Fig. 5 Classification of the pathological ^{1}H-MR spectra based on determination of the main metabolites, namely *N*-acetylaspartate (*NAA*), choline-containing compounds (*Cho*), lactate (*Lac*), and mobile lipids (*Lip*). Types IC and IIC are further subdivided in cases with mild and moderate elevation of Lip. Types IIIB and IIIC are typical for necrotic lesions (*Source*: Chernov et al. [10])

ventricles or bone structures may create significant technical obstacles to spectroscopic investigation.

Single Photon Emission Computed Tomography

Single photon emission computed tomography (SPECT) is based on detection of tracers labeled with gamma-emitting isotopes by rotating scintillation detectors (gamma cameras). To evaluate progressing brain tumors after radiosurgery, several investigators have used thallium-201 chloride (^{201}Tl), the uptake of which is related to CBF, BBB alterations, and variability of Na/K-ATPase pump expression. Using ^{201}Tl SPECT, Serizawa et al. [74] prospectively evaluated 72 brain metastases that were enlarging after GKS. Tumor recurrence was diagnosed if the Tl index (ratio of the radioisotope activity in the tumor relative to that of normal brain tissue) was >5, whereas radiation injury was considered present if it was <3. If the Tl index was between 3 and 5, the investigation was repeated in 1 month (which was required for 57 % of the lesions). Using their criteria the authors found 90 % diagnostic accuracy for differentiating tumor recurrence from radiation injury. In another study, using a cutoff level for Tl index of 2.5, Kimura et al. [43] established the correct diagnosis in 74 % of patients with brain metastases that demonstrated enlargement after SRS.

Others, however, claimed that ^{201}Tl SPECT is a sensitive but relatively nonspecific modality for identifying progressing tumors after irradiation, and that its spatial resolution is too low (8–10 mm). False-positive and false-negative results were reported [20, 40, 71, 74, 79]. Nonneoplastic lesions with BBB disruption (radiation-induced necrosis, inflammation, infarct) as well as hematomas and abscesses may display increased ^{201}Tl uptake. The risk of diagnostic error is particularly high for small tumors and masses located infratentorially or in the vicinity of brain structures with high physiological tracer uptake (e.g., orbit, choroid plexus, hypophyseal region). False-negative results may be caused by administration of steroids [74]. In the series of Tsuyuguchi et al. [79] 81 % of brain metastases enlarging after SRS showed accumulation of ^{201}Tl, but no significant

difference was noted between the recurrence and necrosis groups. A review of studies on the use of ^{201}Tl SPECT for evaluating recurrent supratentorial gliomas after radiotherapy revealed that the sensitivity and specificity of the method vary widely: 43–100 % and 25–100 %, respectively [80]. Use of double isotope investigations (e.g., ^{201}Tl and ^{99m}Tc-HMPAO) or delayed scanning may result in greater diagnostic effectiveness of SPECT [77, 79].

Positron Emission Tomography

Among the diagnostic modalities used to differentiate tumor progression from radiation-induced necrosis, positron emission tomography (PET) has probably obtained the widest acceptance. Hypermetabolic tumor cells actively accumulate radioisotope tracer, whereas hypometabolic necrosis does not, which theoretically leads to a straightforward diagnosis (Fig. 6). Indeed, initial studies with the use of ^{18}F-fluorodeoxyglucose (FDG)-PET showed high efficacy for identifying recurrent brain tumors after irradiation [5, 6, 42, 50, 81, 85]. The reported sensitivity and specificity of the method for identifying recurrent brain metastases after SRS were 65–82 % and 80–97 %, respectively [6, 81]. The diagnostic accuracy was further improved by co-registration of the metabolic data with structural MRI and/or a computerized brain atlas [6, 81]. However, erroneous results of FDG-PET regarding identification of progressing neoplasms are not uncommon [40, 71]. Small tumors, reduced metabolic rate or predominantly anaerobic metabolism, and low resolution may cause false-negative results, whereas high radioisotope uptake in the normal cortex and basal ganglia, areas of inflammation, or epileptic foci may lead to false-positive findings [11, 25, 50]. Additionally, glucose metabolism is affected by steroid therapy [25]. Greater efficacy of FDG-PET in identifying recurrent brain tumors seemingly can be attained with initial glucose loading, delayed imaging, and dual phase investigations [29, 73], but the clinical usefulness of such techniques require further evaluation.

In contrast to FDG, the background uptake of radioisotopes based on aminoacids (e.g., L-methyl-^{11}C-methionine [MET]) in normal brain tissue is low (beside the pons), which may provide optimal visualization of the neoplasm. MET-PET showed high effectiveness in differentiating recurrent intracranial metastases and gliomas from radiation-induced necrosis after SRS or radiotherapy [76, 79]. Using a tumor/normal tissue ratio cutoff value of 1.42 Tsuyuguchi et al. [79] found 78 % sensitivity and 100 % specificity for identification of progressing metastases after SRS. The mechanisms of MET accumulation in the tumor are not clear but may be related to increased protein synthesis by proliferating cells, active transport of amino acid across the cell membrane, BBB disruption, and high vascular density. Its uptake rates correlate with immunopositivity to MIB-1 and PCNA [25]. Nevertheless, increased accumulation of MET is seen occasionally in intracerebral hematomas, areas of inflammation, reactive gliosis, and radiation-induced necrosis [76, 79].

There is continuing search for new tracers for PET, which can provide highly specific and sensitive identification of recurrent intracranial tumors. This list includes, but is not limited to, radioisotopes based on fluoroethyltyrosine (FET), fluorothymidine (FLT), fluoro-L-dihydroxyphenylalanine (FDOPA), and acetate [8, 25, 28, 52, 67]. However, they are generally not available for routine clinical practice, so their diagnostic usefulness in progressing lesions after SRS has not been clarified.

Comparative Evaluation of the Various Diagnostic Modalities

It is evident that functional and metabolic neuroimaging is helpful for diagnosing brain tumor recurrence after irradiation and for differentiating it from treatment-induced effects. It remains unclear, however, which modality provides superior diagnostic accuracy. Despite some comparative studies on this matter, reliable information remains scarce.

Several investigations demonstrated lower diagnostic performance of FDG-PET compared to multivoxel ^{1}H-MRS and MET-PET in cases of brain metastases progressing after SRS [11, 79]; compared to ^{201}Tl-SPECT, MET-, FLT-, and FDOPA-PET in cases of recurrent gliomas, particularly low-grade tumors [8, 28, 76]; and compared to acetate-PET for evaluating the response of meningiomas to GKS [52]. On the other hand MET-PET seems more efficient than ^{201}Tl-SPECT for identifying brain metastases that are progressing after SRS [79], and it provides results comparable to those achieved with FET-PET in recurrent gliomas [67]. In cases of brain metastases progressing after irradiation, the diagnostic accuracy of perfusion MRI is better than that of multivoxel ^{1}H-MRS [30], which in turn is slightly more effective than ^{201}Tl-SPECT [43]. Finally, multivoxel ^{1}H-MRS is somewhat more accurate than DWI with ADC measurements for identifying recurrent gliomas [69].

It should be kept in mind that various radiological modalities provide complementary information on irradiated intracranial masses, which justifies use of a multimodal diagnostic approach [30, 33, 49, 50, 59, 60, 69]. Spatial and temporal discordances are common with multiparametric imaging. Therefore, only by combining data derived from several techniques can we arrive at a unique multifaceted characterization of the lesion [59]. In 2006, our group proposed an

Fig. 6 T1-weighted (*left*) and T2-weighted (*center*) MRI and ^{18}F-fluorodeoxyglucose–positron emission tomography (FDG-PET) (*right*) of a metastatic adenocarcinoma in the left cerebellar hemisphere progressing after GKS (*Source*: Chernov et al. [11])

algorithm for differentiating tumor recurrence from treatment-induced effects after GKS of metastatic brain tumors. The algorithm was based on multivoxel ^{1}H-MRS and PET [12]. Its updated version is presented on Fig. 7, but the efficacy of this diagnostic strategy still requires detailed clinical evaluation.

Role of Serial Functional and Metabolic Imaging After Radiosurgery

Application of serial functional and metabolic evaluations during follow-up provides detailed information on the radiosurgery-induced pathophysiological reactions within the target [59]. DWI, PWI, and ^{1}H-MRS, seem particularly attractive because they can be applied with relative ease at the time of a routine MRI investigation. It was shown that successful radiosurgery results in a gradually increasing ADC [23, 31, 78] and decreased relative CBF [82, 83] and CBV [17] in patients with a metastatic brain tumor. Longitudinal spectroscopic changes in such cases are complex as the initial decrease in Cho, Lac, and Lip peak intensities reflect apoptotic cell loss and inhibition of tumor metabolism. An increase of these metabolites is characteristic of early necrotic changes, whereas further development of radiation-induced necrosis is associated with a decrease in Cho and further elevation of Lac and Lip or, in the late stage, even disappearance of all metabolite peaks [9, 43, 44, 46, 49, 51, 66, 82, 85]. An increase in the neuronal marker NAA usually accompanies tumor shrinkage but sometimes is evident even before initiation of volumetric changes [9]. It is possible that similar dynamics, although of lesser magnitude, of DWI-, PWI-, and ^{1}H-MRS-related parameters can also be observed after SRS of benign extracerebral tumors [46, 78].

Such changes may precede tumor shrinkage or even be detected at the time of mass enlargement. Hence, there is a promising potential to evaluate the effect of treatment long before a measurable response is detected [17, 23, 31, 43, 78, 83]. On the other hand, opposite dynamics usually accompany recurrence or regrowth of the neoplasm. Theoretically, serial functional and metabolic imaging can predict progression of the tumor before there is definite increase in its volume [9, 23, 31, 43, 78]. In the series of Goldman et al. [23], all of the brain metastases for which shrinkage after GKS was not accompanied by a significant increase in the ADC invariably recurred. Increased relative CBF and CBV at 6 weeks after SRS of brain metastases compared to the pretreatment level accurately predicted subsequent tumor progression [17, 83]. Our serial ^{1}H-MRS investigations of intracranial metastases after radiosurgery [9] revealed several subtle neurochemical alterations preceding definite regrowth of the neoplasm (Fig. 8). Nevertheless, the clinical applicability of this diagnostic approach and its possible usefulness for correcting therapy before evidence of volumetric change in the tumor requires additional validation.

Multiple metabolic assessments by means of SPECT or PET are difficult because of the need of special equipment, necessity of injecting radioactive isotopes, and cost of investigation. Nevertheless, Serizawa et al. [74] performed serial ^{201}Tl-SPECT of 41 brain metastases that had enlarged after radiosurgery. They found that tumor recurrence was typically associated with a steadily increasing Tl index, whereas in cases of radiation injury it had a fluctuating course. Based on their experience, the authors defined three metabolic responses after GKS: (1) good—with a prominent decrease in the Tl index within 1 month after SRS and continuous reduction thereafter; (2) early recurrence—with a prominent decrease in the Tl index within 1 month after SRS and steady increase thereafter; (3) poor—with a moderate decrease in the Tl index within

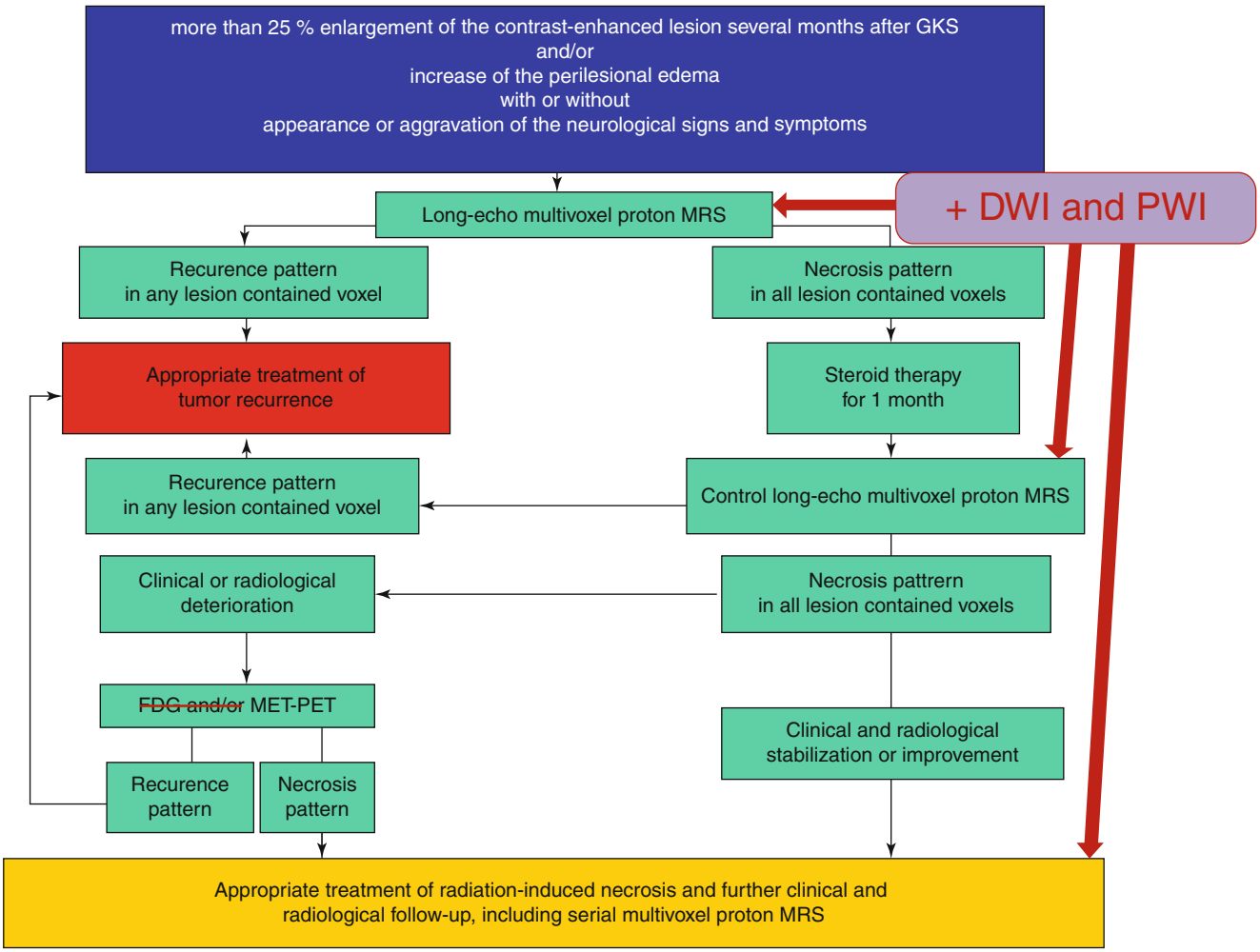

Fig. 7 Diagnostic algorithm for differentiating tumor recurrence from radiation-induced necrosis after irradiation of metastatic brain tumors (modified from Chernov et al. [12]). Compared to the previous version, diffusion-weighted (DWI) and perfusion-weighted (PWI) imaging are added to multivoxel ^{1}H-MRS, whereas FDG-PET is eliminated. *GKS* Gamma Knife radiosurgery

1 month after SRS and its fluctuation thereafter [74]. Tomura et al. [77] revealed that a decrease in the Tl index within the first week after stereotactic irradiation of various intracranial tumors is highly predictive of a subsequent volumetric response. Yoshino et al. [85] performed serial fluoroboronophenylalanine (FBPA)-PET and FDG-PET in a few patients after GKS on brain metastases and found a steady decrease of radioisotope uptake somewhat preceding and accompanying tumor shrinkage. Enlargement of the lesion caused by radiation-induced necrosis was not accompanied by metabolic changes. The similar findings on serial FDG-PET were noted previously after radiosurgery of intracranial meningiomas [62]. However, recently Liu et al. [52] compared acetate-PET and FDG-PET before and after GKS of these tumors. The former tracer showed reduced uptake after irradiation and predicted a volumetric response, but FDG accumulation was nonspecifically increased after irradiation in some cases, which was probably caused by temporary BBB alteration.

In general, it is clear that addition of functional and metabolic investigations to structural MRI during regular follow-up after intracranial radiosurgery allows detailed evaluation of the time-evolving treatment effects and assessment of their dynamics. However, the clinical significance of the obtained information should be defined in further studies.

Tissue Sampling of Lesions Progressing After Radiosurgery

Tissue investigation still represents the gold standard for precise characterization of brain lesions progressing after irradiation. However, the histopathological diagnosis can be challenging, especially if performed on small biopsy

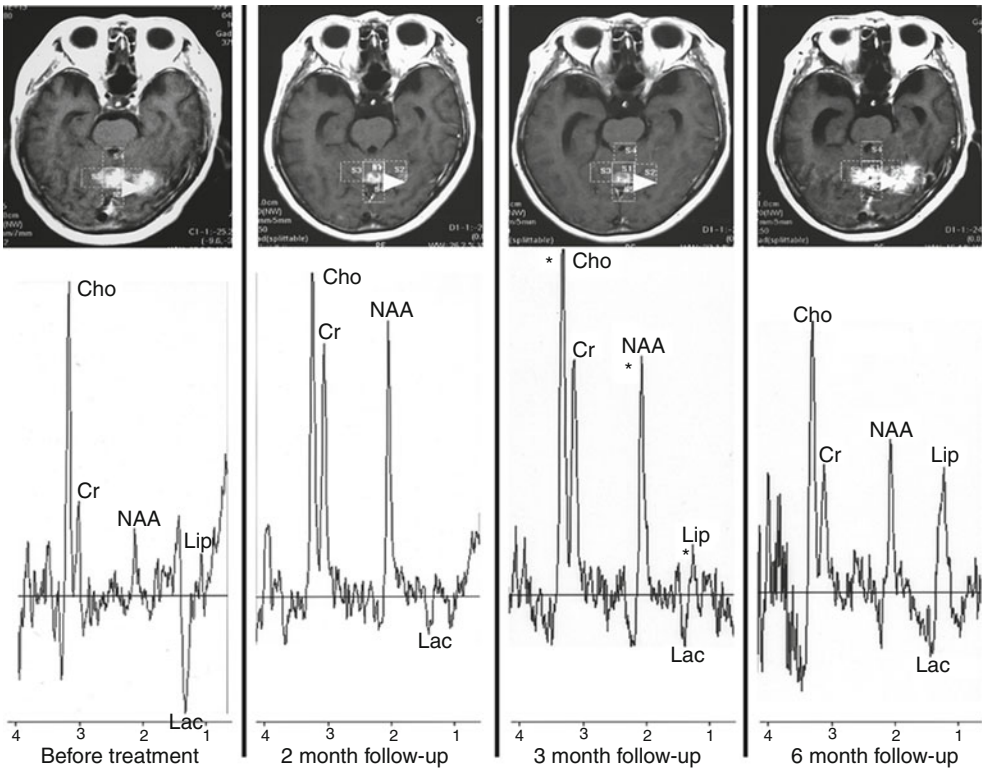

Fig. 8 ^{1}H-MRS-detected metabolic changes in an intracranial metastasis of breast cancer that initially showed prominent volume reduction but recurred at 6 months after GKS. Note the presence of a mild increase in choline-containing compounds (*Cho*) and mobile lipids (*Lip*) and a decrease in *N*-acetylaspartate (*NAA*) at the 3-month follow-up before an increase in tumor volume (*asterisks*). At the time of volumetric lesion progression, there was some decrease in *Cho* accompanied by an evident decrease in *NAA* and creatine (*Cr*) and an increase in *Lip*. *Lac* lactate (*Source*: Chernov et al. [9])

specimens. Various radiation-induced changes may be intermixed with the neoplastic elements, or they may predominate in different parts of the mass. Identification of tumor cells on the background of necrosis may raise a question on their viability and proliferative potential. False-positive results of MIB-1 immunostaining in quiescent tumors after SRS have been reported [37]. As improved tissue sampling can significantly facilitate a histopathological diagnosis, functional or metabolic guidance with PWI, ^{1}H-MRS, or MET-PET and/or neurochemical navigation with 5-aminolevulinic acid seem quite reasonable in such cases during stereotactic biopsy or open microsurgical resection.

Limitations of the Available Studies

The majority of available studies evaluating the various neuroimaging modalities for identification and characterization of brain tumor progression after irradiation suffer from significant methodological shortcomings. Thus, we must be extremely careful when interpreting their results. The main pitfalls typically include a retrospective design and a relatively small number of cases, which does not allow reliable determination of the specific cutoff levels and thresholds of the various diagnostic parameters. In many cases, the final decision on the nature of pathology is based not on the histopathological examination but on reliance on some neuroimaging modality defined as the gold standard or on a stable clinical course, the durations of which varied from one series to another. If tissue sampling was performed, the tissue was frequently obtained by stereotactic biopsy. Hence, the obtained specimen might not be representative of the whole lesion. Such inconsistencies result in significant variability of the reported diagnostic efficacy of the methods. Moreover, the absence of standard methodologies for functional and metabolic investigations and the differences in the equipment, methods of data evaluation (qualitative, semiquantitative, quantitative) and investigated parameters (mean, maximum, and various normalized values using subjectively defined ROIs) do not permit straightforward comparison of the results obtained in separate centers. These shortcomings create significant challenges for directly introducing the reported techniques into clinical practice without preliminary testing and validation.

Future Perspectives

Introduction of the multimodal diagnostic approach requires development of optimized radiological protocols for differentiating tumor progression from radiation-induced changes after SRS. The growing availability of multidetector CT and high magnetic field MRI scanners, the development of new

MRI sequences, and the search for more effective contrast media and radioisotope tracers will significantly extend diagnostic options. Further advances of the fusion techniques and hybrid imaging (e.g., PET-CT, PET-MRI) will improve effective lesion characterization, particularly when using methods with limited spatial resolution. Frequent coexistence of the viable neoplastic elements and postirradiation changes should encourage studies directed at evaluating their relative representation within the same lesion based on quantitative assessment of the heterogeneity of the radiological findings relevant to the histopathology and clinical course. Possible usefulness of serial functional and metabolic neuroimaging starting before SRS and continuing during the subsequent follow-up for early prediction of response to treatment and timely identification of tumor progression should be tested prospectively with strict predetermined diagnostic criteria and outcome measures. These investigations will require development of advanced software workspaces for integrated cross-correlated computer-aided analysis of the multiple data undergoing spatial and temporal changes [59]. Wide introduction of the results of such studies into routine clinical practice cannot be attained without technical standardization of the advanced neuroimaging modalities (e.g., perfusion MRI, ^{1}H-MRS). Finally, development of molecular imaging techniques, particularly those based on amide proton transfer MRI [36], may result in very effective noninvasive characterization of brain lesions after irradiation. Their practical application in the future seems promising.

Conclusion

Differentiation of tumor progression from radiation-induced effects after intracranial radiosurgery is challenging. It includes complex evaluation of various clinical, radiosurgical, and radiological factors. Evaluating volumetric changes by structural contrast-enhanced MRI seems sufficient after low-dose SRS of benign intracranial tumors. In such cases possible delayed growth arrest and transitory enlargement of the lesion should be always borne in mind, because usually they do not require additional treatment. Multimodal neuroimaging with application of the various functional and metabolic techniques is preferable in diagnostically difficult cases. Addition of DWI, perfusion studies, and ^{1}H-MRS to regular structural MRI investigations during follow-up after SRS of parenchymal brain tumors allows detailed longitudinal assessment of the treatment effects and, along with MET PET, provides valuable diagnostic information about progressing lesions. Finally, it should be kept in mind that differentiating tumor recurrence from radiation-induced effects after SRS does not indicate whether to apply surgical treatment or reserve it. In fact, resection of the lesion may be required for either condition. If indicated, it should be performed under metabolic guidance.

Conflict of Interest The authors declare that they have no conflict of interest. The research activities of Dr. Mikhail Chernov during 2010–2012 were supported by the Japan Society for the Promotion of Science (JSPS; ID No. P 10128).

References

1. Asao C, Korogi Y, Kitajima M, Hirai T, Baba Y, Makino K, Kochi M, Morishita S, Yamashita Y (2005) Diffusion-weighted imaging of radiation-induced brain injury for differentiation from tumor recurrence. AJNR Am J Neuroradiol 26:1455–1460
2. Barajas RF, Chang JS, Sneed PK, Segal MR, McDermott MW, Cha S (2009) Distinguishing recurrent intra-axial metastatic tumor from radiation necrosis following Gamma Knife radiosurgery using dynamic susceptibility-weighted contrast-enhanced perfusion MR imaging. AJNR Am J Neuroradiol 30:367–372
3. Blonigen BJ, Steinmetz RD, Levin L, Lamba MA, Warnick RE, Breneman JC (2010) Irradiated volume as a predictor of brain radionecrosis after linear accelerator stereotactic radiosurgery. Int J Radiat Oncol Biol Phys 77:996–1001
4. Brismar J, Roberson GH, Davis KR (1976) Radiation necrosis of the brain. Neuroradiological considerations with computed tomography. Neuroradiology 12:109–113
5. Castel JC, Caille JM (1989) Imaging of irradiated brain tumours: value of magnetic resonance imaging. J Neuroradiol 16:81–132
6. Chao ST, Suh JH, Raja S, Lee SY, Barnett G (2001) The sensitivity and specificity of FDG PET in distinguishing recurrent brain tumor from radionecrosis in patients treated with stereotactic radiosurgery. Int J Cancer 96:191–197
7. Chen HI, Burnett MG, Huse JT, Lustig RA, Bagley LJ, Zager EL (2006) Recurrent late cerebral necrosis with aggressive characteristics after radiosurgical treatment of an arteriovenous malformation. J Neurosurg 105:455–460
8. Chen W, Silverman DH, Delaloye S, Czernin J, Kamdar N, Pope W, Satyamurthy N, Schiepers C, Cloughesy T (2006) 18F-FDOPA PET imaging of brain tumors: comparison study with 18F-FDG PET and evaluation of diagnostic accuracy. J Nucl Med 47:904–911
9. Chernov MF, Hayashi M, Izawa M, Nakaya K, Tamura N, Ono Y, Abe K, Usukura M, Yoshida S, Nakamura R, Suzuki T, Muragaki Y, Iseki H, Kubo O, Hori T, Takakura K (2009) Dynamics of metabolic changes in intracranial metastases and distant normal-appearing brain tissue after stereotactic radiosurgery: a serial proton magnetic resonance spectroscopy study. Neuroradiol J 22:58–71
10. Chernov M, Hayashi M, Izawa M, Nakaya K, Ono Y, Usukura M, Yoshida S, Kato K, Muragaki Y, Nakamura R, Iseki H, Hori T, Takakura K (2007) Metabolic characteristics of intracranial metastases, detected by single-voxel proton magnetic resonance spectroscopy, are seemingly not predictive for tumor response to gamma knife radiosurgery. Minim Invasive Neurosurg 50:233–238
11. Chernov MF, Hayashi M, Izawa M, Ochiai T, Usukura M, Abe K, Ono Y, Muragaki Y, Kubo O, Hori T, Takakura K (2005) Differentiation of the radiation-induced necrosis and tumor recurrence after Gamma Knife radiosurgery for brain metastases: importance of multi-voxel proton MRS. Minim Invasive Neurosurg 48:228–234

12. Chernov MF, Hayashi M, Izawa M, Usukura M, Yoshida S, Ono Y, Muragaki Y, Kubo O, Hori T, Takakura K (2006) Multivoxel proton MRS for differentiation of radiation-induced necrosis and tumor recurrence after Gamma Knife radiosurgery for brain metastases. Brain Tumor Pathol 23:19–27
13. Chin LS, Ma L, DiBiase S (2001) Radiation necrosis following Gamma Knife surgery: a case-controlled comparison of treatment parameters and long-term clinical follow-up. J Neurosurg 94:899–904
14. Couldwell WT, Cole CD, Al-Mefty O (2007) Patterns of skull base meningioma progression after failed radiosurgery. J Neurosurg 106:30–35
15. Delsanti C, Roche PH, Thomassin JM, Regis J (2008) Morphological changes of vestibular schwannomas after radiosurgical treatment: pitfalls and diagnosis of failure. In: Regis J, Roche PH (eds) Modern Management of Acoustic Neuroma. Prog Neurol Surg, vol. 21. Karger, Basel, pp 93–97
16. Dequesada IM, Quisling RG, Yachnis A, Friedman WA (2008) Can standard magnetic resonance imaging reliably distinguish recurrent tumor from radiation necrosis after radiosurgery for brain metastases? A radiographic-pathological study. Neurosurgery 63:898–904
17. Essig M, Waschkies M, Wenz F, Debus J, Hentrich HR, Knopp MV (2003) Assessment of brain metastases with dynamic susceptibility-weighted contrast-enhanced MR imaging: initial results. Radiology 228:193–199
18. Feigl GC, Horstmann GA (2006) Volumetric follow up of brain metastases: a useful method to evaluate treatment outcome and predict survival after Gamma Knife surgery? J Neurosurg 105(Suppl):91–98
19. Feigl GC, Samii M, Horstman GA (2007) Volumetric follow-up of meningiomas: a quantitative method to evaluate treatment outcome of gamma knife radiosurgery. Neurosurgery 61:281–287
20. Foroughi M, Kemeny AA, Lehecka M, Wons J, Kajdi L, Hatfield R, Marks S (2010) Operative intervention for delayed symptomatic radionecrotic masses developing following stereotactic radiosurgery for cerebral arteriovenous malformations – case analysis and literature review. Acta Neurochir (Wien) 152:803–815
21. Ganz JC, Reda WA, Abdelkarim K (2009) Adverse radiation effects after Gamma Knife surgery in relation to dose and volume. Acta Neurochir (Wien) 151:9–19
22. Gao X, Zhang XN, Zhang YT, Yu CS, Xu DS (2011) Magnetic resonance imaging in assessment of treatment response of Gamma Knife for brain tumors. Chin Med J (Engl) 124:1906–1910
23. Goldman M, Boxerman JL, Rogg JM, Noren G (2006) Utility of apparent diffusion coefficient in predicting the outcome of gamma knife-treated brain metastases prior to changes in tumor volume: a preliminary study. J Neurosurg 105(Suppl):175–182
24. Hasegawa T, Kida Y, Yoshimoto M, Koike J, Goto K (2006) Evaluation of tumor expansion after stereotactic radiosurgery in patients harboring vestibular schwannomas. Neurosurgery 58: 1119–1128
25. Herholz K, Coope D, Jackson A (2007) Metabolic and molecular imaging in neuro-oncology. Lancet Neurol 6:711–724
26. Hirato M, Hirato J, Zama A, Inoue H, Ohye C, Shibazaki T, Andou Y (1996) Radiobiological effects of gamma knife radiosurgery on brain tumors studied in autopsy and surgical specimens. Stereotact Funct Neurosurg 66(Suppl 1):4–16
27. Hoefnagels FWA, Lagerwaard FJ, Sanchez E, Haasbeek CJA, Knol DL, Slotman BJ, Vandertop WP (2009) Radiological progression of cerebral metastases after radiosurgery: assessment of perfusion MRI for differentiating between necrosis and recurrence. J Neurol 256:878–887
28. Hong IK, Kim JH, Ra YS, Kwon DH, Oh SJ, Kim JS (2011) Diagnostic usefulness of 3′-deoxy-3′-[18F] fluorothymidine positron emission tomography in recurrent brain tumor. J Comput Assist Tomogr 35:679–684
29. Horky LL, Hsiao EM, Weiss SE, Drappatz J, Gerbaudo VH (2011) Dual phase FDG-PET imaging of brain metastases provides superior assessment of recurrence versus post-treatment necrosis. J Neurooncol 103:137–146
30. Huang J, Wang AM, Shetty A, Maitz AH, Yan D, Doyle D, Richey K, Park S, Pieper DR, Chen PY, Grills IS (2011) Differentiation between intra-axial metastatic tumor progression and radiation injury following fractionated radiation therapy or stereotactic radiosurgery using MR spectroscopy, perfusion MR imaging or volume progression modeling. Magn Reson Imaging 29: 993–1001
31. Huang CF, Chou HH, Tu HT, Yang MS, Lee JK, Lin LY (2008) Diffusion magnetic resonance imaging as an evaluation of the response of brain metastases treated by stereotactic radiosurgery. Surg Neurol 69:62–68
32. Jagannathan J, Bourne TD, Schlesinger D, Yen CP, Shaffrey ME, Laws ER Jr, Sheehan JP (2010) Clinical and pathological characteristics of brain metastases resected after failed radiosurgery. Neurosurgery 66:208–217
33. Jain R, Narang J, Schultz L, Scarpace L, Saksena S, Brown S, Rock JP, Rosenblum M, Gutierrez J, Mikkelsen T (2011) Permeability estimates in histopathology-proved treatment-induced necrosis using perfusion CT: can these add to other perfusion parameters in differentiating from recurrent/progressive tumors? AJNR Am J Neuroradiol 32:658–663
34. Jain R, Narang J, Sundgren PM, Hearshen D, Saksena S, Rock JP, Gutierrez J, Mikkelsen T (2010) Treatment induced necrosis versus recurrent/progressing brain tumor: going beyond the boundaries of conventional morphologic imaging. J Neurooncol 100:17–29
35. Jain R, Scarpace L, Ellika S, Schultz LR, Rock JP, Rosenblum ML, Patel SC, Lee TY, Mikkelsen T (2007) First-pass perfusion computed tomography: initial experience in differentiating recurrent brain tumors from radiation effects and radiation necrosis. Neurosurgery 61:778–787
36. Jandial R, Duenas VJ, Chen BT (2011) Molecular imaging based on differential protein content in differentiating glioma from radiation necrosis. Neurosurgery 68(6):N16–N17
37. Jennelle R, Gladson C, Palmer C, Guthrie B, Markert J (1999) Paradoxical labeling of radiosurgically treated quiescent tumors with Ki 67, a marker of cellular proliferation. Stereotact Funct Neurosurg 72(Suppl 1):45–52
38. Kamada K, Mastuo T, Tani M, Izumo T, Suzuki Y, Okimoto T, Hayashi N, Hyashi K, Shibata S (2001) Effects of stereotactic radiosurgery on metastatic brain tumors of various histopahtologies. Neuropathology 21:307–314
39. Kang TW, Kim ST, Byun HS, Jeon P, Kim K, Kim H, Lee J II (2009) Morphological and functional MRI, MRS, perfusion and diffusion changes after radiosurgery of brain metastasis. Eur J Radiol 72:370–380
40. Kano H, Kondziolka D, Lobato-Polo J, Zorro O, Flickinger JC, Lunsford LD (2010) Differentiating radiation effect from tumor progression after stereotactic radiosurgery: T1/T2 matching. Clin Neurosurg 57:160–165
41. Kano H, Kondziolka D, Lobato-Polo J, Zorro O, Flickinger JC, Lunsford LD (2010) T1/T2 matching to differentiate tumor growth from radiation effects after stereotactic radiosurgery. Neurosurgery 66:486–492
42. Kihlstrom L, Karlsson B (1999) Imaging changes after radiosurgery for vascular malformations, functional targets and tumors. Neurosurg Clin N Am 10:167–180
43. Kimura T, Sako K, Tanaka K, Gotoh T, Yoshida H, Aburano T, Tanaka T, Arai H, Nakada T (2004) Evaluation of the response of metastatic brain tumors to stereotactic radiosurgery by proton magnetic resonance spectroscopy, ^{201}TlCl single-photon emission computerized tomography, and gadolinium-enhanced magnetic resonance imaging. J Neurosurg 100:835–841

44. Kimura T, Sako K, Tohyama Y, Aizawa S, Yoshida H, Aburano T, Tanaka K, Tanaka T (2003) Diagnosis and treatment of progressive space-occupying radiation necrosis following stereotactic radiosurgery for brain metastases: value of proton magnetic resonance spectroscopy. Acta Neurochir (Wien) 145:557–564
45. Kingsley DP, Kendall BE (1981) CT of the adverse effects of therapeutic radiation of the Central Nervous System. AJNR Am J Neuroradiol 2:453–460
46. Kizu O, Naruse S, Furuya S, Morishita H, Ide M, Maeda T, Ueda S (1998) Application of proton chemical shift imaging in monitoring of gamma knife radiosurgery on brain tumors. Magn Reson Imaging 16:197–204
47. Korytko T, Radivoyevitch T, Colussi V, Wessels BW, Pillai K, Maciunas RJ, Einstein DB (2006) 12 Gy gamma knife radiosurgical volume is a predictor for radiation necrosis in non-AVM intracranial tumors. Int J Radiat Oncol Biol Phys 64:419–424
48. Kubo O, Chernov M, Izawa M, Hayashi M, Muragaki Y, Maruyama T, Hori T, Takakura K (2005) Malignant progression of benign brain tumors after gamma knife radiosurgery: is it really caused by irradiation? Minim Invasive Neurosurg 48:334–339
49. Kwock L, Smith JK, Castillo M, Ewend MG, Cush S, Hensing T, Varia M, Morris D, Bouldin TW (2002) Clinical applications of proton MR spectroscopy in oncology. Technol Cancer Res Treat 1:17–28
50. Langleben DD, Segall GM (2000) PET in differentiation of recurrent brain tumor from radiation injury. J Nucl Med 41:1861–1867
51. Lee PL, Gonzalez RG (2000) Magnetic resonance spectroscopy of brain tumors. Curr Opin Oncol 12:199–204
52. Liu RS, Chang CP, Guo WY, Pan DHC, Ho DMT, Chang CW, Yang BH, Wu LC, Yeh SH (2010) 1-^{11}C-Acetate versus ^{18}F-FDG PET in detection of meningioma and monitoring the effect of gamma-knife radiosurgery. J Nucl Med 51:883–891
53. Loeffler JS, Niemierko A, Chapman PH (2003) Second tumors after radiosurgery: tip of the iceberg or a bump in the road? Neurosurgery 52:1436–1442
54. Lunsford LD, Kondziolka D, Maitz A, Flickinger JC (1998) Black holes, white dwarfs and supernovas: imaging after radiosurgery. Stereotact Funct Neurosurg 70(Suppl 1):2–10
55. Lunsford LD, Niranjan A, Martin J, Sirin S, Kassam A, Kondziolka D, Flickinger JC (2007) Radiosurgery for miscellaneous skull base tumors. In: Szeifert GT, Kondziolka D, Levivier M, Lunsford LD (eds) Radiosurgery and Pathological Fundamentals. Prog Neurol Surg, vol. 20. Karger, Basel, pp 192–205
56. Mitsuya K, Nakasu Y, Horiguchi S, Harada H, Nishimura T, Bando E, Okawa H, Furukawa Y, Hirai T, Endo M (2010) Perfusion weighted magnetic resonance imaging to distinguish the recurrence of metastatic brain tumors from radiation necrosis after stereotactic radiosurgery. J Neurooncol 99:81–88
57. Mullins ME, Barest GD, Schaefer PW, Hochberg FH, Gonzalez RG, Lev MH (2005) Radiation necrosis versus glioma recurrence: conventional MR imaging clues to diagnosis. AJNR Am J Neuroradiol 26:1967–1972
58. Niranjan A, Kondziolka D, Lunsford LD (2009) Neoplastic transformation after radiosurgery or radiotherapy: risk and realties. Otolaryngol Clin North Am 42:717–729
59. Padhani AR, Miles KA (2010) Multiparametric imaging of tumor response to therapy. Radiology 256:348–364
60. Palumbo B (2008) Brain tumour recurrence: brain single-photon emission computerized tomography, PET and proton magnetic resonance spectroscopy. Nucl Med Commun 29:730–735
61. Pamir MN, Kilic T, Belirgen M, Abacioglu U, Karabekiroglu N (2007) Pituitary adenomas treated with gamma knife radiosurgery: volumetric analysis of 100 cases with minimum 3 year follow-up. Neurosurgery 61:270–280
62. Pan DHC, Guo WY, Chung WY, Shiau CY, Liu RS, Lee LS (1995) Early effects of gamma knife surgery on malignant and benign intracranial tumors. Stereotact Funct Neurosurg 64(Suppl 1):19–31
63. Patel TR, McHugh BJ, Bi WL, Minja FJ, Knisely JPS, Chiang VL (2011) A comprehensive review of MR imaging changes following radiosurgery to 500 brain metastases. AJNR Am J Neuroradiol 32:1885–1892
64. Plowman PN (1999) Stereotactic radiosurgery VIII. The classification of postirradiation reactions. Br J Neurosurg 13: 256–264
65. Pollock BE (2006) Management of vestibular schwannomas that enlarge after stereotactic radiosurgery: treatment recommendations based on a 15 year experience. Neurosurgery 58:241–248
66. Pruzincova L, Steno J, Srbecky M, Kalina P, Rychly B, Boljesikova E, Chorvath M, Novotny M, Procka V, Makaiova I, Belan V (2009) MR imaging of late radiation therapy- and chemotherapy-induced injury: a pictorial essay. Eur Radiol 19:2716–2727
67. Rachinger W, Goetz C, Popperl G, Gildehaus FJ, Kreth FW, Holtmannspotter M, Herms J, Koch W, Tatsch K, Tonn JC (2005) Positron emission tomography with *O*-(2-[^{18}F]fluoroethyl)-L-Tyrosine versus magnetic resonance imaging in the diagnosis of recurrent gliomas. Neurosurgery 57:505–511
68. Rock JP, Hearshen D, Scarpace L, Croteau D, Gutierrez J, Fisher JL, Rosenblum ML, Mikkelsen T (2002) Correlations between magnetic resonance spectroscopy and image-guided histopathology, with special attention to radiation necrosis. Neurosurgery 51:912–920
69. Rock JP, Scarpace L, Hearshen D, Gutierrez J, Fisher JL, Rosenblum ML, Mikkelsen T (2004) Associations among magnetic resonance spectroscopy, apparent diffusion coefficients, and image-guided histopathology with special attention to radiation necrosis. Neurosurgery 54:1111–1119
70. Rogers LR, Gutierrez J, Scarpace L, Schultz L, Ryu S, Lord B, Movsas B, Nonsowetz J, Jain R (2011) Morphologic magnetic resonance imaging features of therapy-induced cerebral necrosis. J Neurooncol 101:25–32
71. Ross DA, Sandler HM, Balter JM, Hayman JA, Archer PG, Auer DL (2002) Imaging changes after stereotactic radiosurgery of primary and secondary malignant brain tumors. J Neurooncol 56:175–181
72. Rowe J, Grainger A, Walton L, Silcocks P, Radatz M, Kemeny A (2007) Risk of malignancy after gamma knife stereotactic radiosurgery. Neurosurgery 60:60–66
73. Seo YS, Chung TW, Kim IY, Bom HS, Min JJ (2008) Enhanced detectability of recurrent brain tumor using glucose-loading F-18 FDG PET. Clin Nucl Med 33:32–33
74. Serizawa T, Saeki N, Higuchi Y, Ono J, Matsuda S, Sato M, Yanagisawa M, Iuchi T, Nagano O, Yamaura A (2005) Diagnostic value of thallium-201 chloride single-photon emission computerized tomography in differentiating tumor recurrence from radiation injury after Gamma Knife surgery for metastatic brain tumors. J Neurosurg 102(Suppl):266–271
75. Sundgren PC, Fan X, Weybright P, Welsh RC, Carlos RC, Petrou M, McKeever PE, Chenevert TL (2006) Differentiation of recurrent brain tumor versus radiation injury using diffusion tensor imaging in patients with new contrast-enhancing lesions. Magn Reson Imaging 24:1131–1142
76. Terakawa Y, Tsuyuguchi N, Iwai Y, Yamanaka K, Higashiyama S, Takami T, Ohata K (2008) Diagnostic accuracy of ^{11}C-Methionine PET for differentiation of recurrent brain tumors from radiation necrosis after radiotherapy. J Nucl Med 49: 694–699
77. Tomura N, Izumi J, Anbai A, Takahashi S, Sakuma I, Omachi K, Kidani H, Sasaki K, Watarai J, Suzuki A, Mizoi K (2005) Thallium-201 SPECT in the evaluation of early effects on brain tumors treated with stereotactic irradiation. Clin Nucl Med 30:83–86
78. Tomura N, Narita K, Izumi JI, Suzuki A, Anbai A, Otani T, Sakuma I, Takahashi S, Mizoi K, Watarai J (2006) Diffusion

changes in a tumor and peritumoral tissue after stereotactic irradiation for brain tumors: possible prediction of treatment response. J Comput Assist Tomogr 30:496–500
79. Tsuyuguchi N, Sunada I, Iwai Y, Yamanaka K, Tanaka K, Takami T, Otsuka Y, Sakamoto S, Ohata K, Goto T, Hara M (2003) Methionine positron emission tomography of recurrent metastatic brain tumor and radiation necrosis after stereotactic radiosurgery: is a differential diagnosis possible? J Neurosurg 98:1056–1064
80. Vos MJ, Tony BN, Hoekstra OS, Postma TJ, Heimans JJ, Hooft L (2007) Systematic review of the diagnostic accuracy of 201Tl single photon emission computed tomography in the detection of recurrent glioma. Nucl Med Commun 28:431–439
81. Wang SX, Boethius J, Ericson K (2006) FDG-PET on irradiated brain tumor: ten years' summary. Acta Radiol 47:85–90
82. Weber MA, Lichy MP, Thilmann C, Gunther M, Bachert P, Maudsley AA, Delorme S, Schad LR, Debus J, Schlemmer HP (2003) Monitoring of irradiated brain metastases using MR perfusion imaging and 1H MR spectroscopy. Radiologe 43:388–395 (in German)
83. Weber MA, Thilmann C, Lichy MP, Gunther M, Delorme S, Zuna I, Bongers A, Schad LR, Debus J, Kauczor HU, Essig M, Schlemmer HP (2004) Assessment of irradiated brain metastases by means of arterial spin-labeling and dynamic susceptibility-weighted contrast-enhanced perfusion MRI: initial results. Invest Radiol 39:277–287
84. Young GS (2007) Advanced MRI of adult brain tumors. Neurol Clin 25:947–973
85. Yoshino E, Ohmori Y, Imahori Y, Higuchi T, Furuya S, Naruse S, Mori T, Suzuki K, Yamaki T, Ueda S, Tsuzuki T, Takai S (1996) Irradaition effects on the metabolism of metastatic brain tumors: analysis by positron emission tomography and ^{1}H-magnetic resonance spectroscopy. Stereotact Funct Neurosurg 66(Suppl 1): 240–259
86. Zada G, Pagnini PG, Yu C, Erickson KT, Hirschbein J, Zelman V, Apuzzo MLJ (2010) Long-term outcomes and patterns of tumor progression after gamma knife radiosurgery for benign meningiomas. Neurosurgery 67:322–329